ELSEVIER

Surface and Coatings Technology 149 (2002) 7–13

SURFACE & COATINGS TECHNOLOGY

www.elsevier.com/locate/surfcoat

Mechanical properties of TiN thin film coatings on 304 stainless steel substrates

Wen-Jun Chou, Ge-Ping Yu, Jia-Hong Huang*

Department of Engineering and System Science, National Tsing Hua University, 101 Kuang Fu Road, section 2, Hsinchu 300, Taiwan, ROC

Received 2 November 2000; accepted in revised form 5 July 2001

Abstract

Titanium nitride (TiN) film was deposited on 304 stainless steel using a hollow cathode discharge ion-plating (HCD-IP) technique. Film thickness and N/Ti ratio were controlled. The depth profile of the composition was determined by secondary ion spectroscopy (SIMS). The results showed that the compositions of the films were uniform for the films deposited at the same deposition conditions. The purpose of this study is to investigate the variation of structure and mechanical properties of the TiN films with different film thickness. The preferred orientations of TiN films were determined using X-ray diffraction (XRD). The dominant preferred orientation of the TiN coatings for the deposition conditions was (111), especially for the films thicker than 1 μm. The residual stress of the TiN films was also measured by XRD using $\sin^2 \Psi$ method. The residual stress was ranging from −5.93 to −2.70 GPa, varying with film thickness. Hardness of the films was measured by nanoindentation. The hardness values were ranging from 14.9 to 33.6 GPa, increasing with the film thickness. The ultimate interfacial shear stress between TiN /304SS was determined by in-situ strip tension of the TiN-coated specimens in a scanning electron microscope (SEM) chamber. The limiting thickness for the effective measurement of interfacial shear strength by the in-situ strip tension method is close to 0.5 μm. N/Ti ratios of the thin films were all at 0.8 measured using both X-ray photoelectron spectrometer (XPS) and Rutherford backscattering spectrometer (RBS). The packing factors of TiN films, calculated from the results of RBS, were 0.62–0.99, increasing with film thickness and leveling off at a thickness above 1.2 μm.

Keywords: TiN; Ion plating; Mechanical properties

1. Introduction

Owing to its superior mechanical properties, titanium nitride (TiN) films are widely utilized in many industrial areas where high abrasion resistance, low friction coefficient, high temperature stability, and high hardness are required. The mechanical properties of TiN are strongly related to its preferred orientation [1,2]. It has been reported [3,4] that TiN film with (111) preferred orientation possess the highest hardness. During the PVD deposition of a thin film, the packing density and preferred orientation of the film normally changes with the increasing film thickness. Therefore, film thickness is an important parameter that affects the preferred orientation and hardness of the coating. In addition, it is known that PVD coated specimens will inevitably have residual stress after the process is complete. The residual stress is also a significant factor for influencing preferred orientation [5,6], adhesion, and hardness [7,8] of the coating.

In order to prolong the service life, a TiN coating is usually chosen as a protective film for many kinds of metal surfaces. One of the major applications of this protective layer is the coating of stainless steels. Stainless steels are widely used in industry and daily life due to their high corrosion and oxidation resistance. By coating with a TiN film, not only the corrosion resistance of stainless steel can be increased, but also the surface

* Corresponding author. Tel.: +886-35715131, (ext.) 4274; fax: +886-35720724.

E-mail address: jhhuang@ess.nthu.edu.tw (J.-H. Huang).

0257-8972/01/$ - see front matter
PII: S0257-8972(01)01382-2

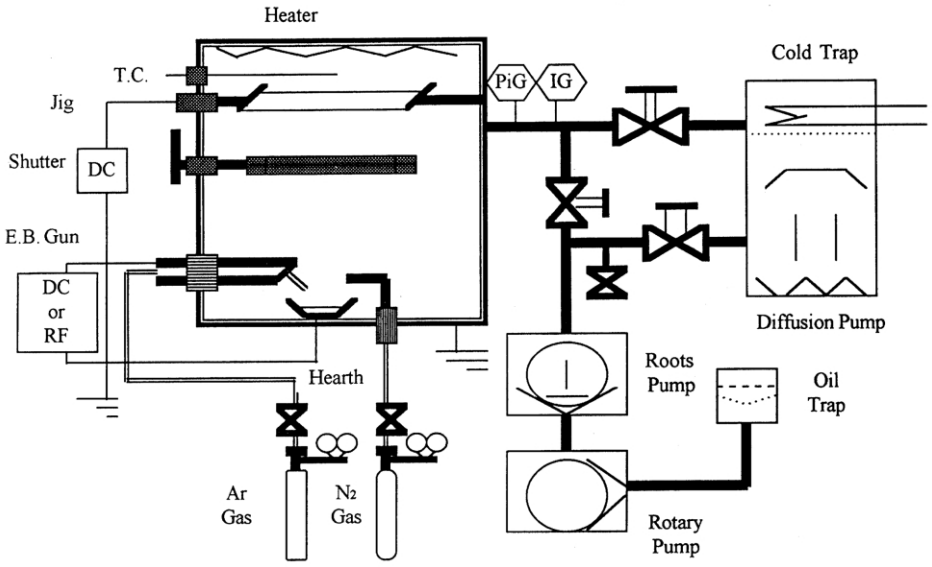

Fig. 1. Schematic diagram of the hollow cathode discharge ion-plating (HCD-IP) system.

hardness is improved, and the golden decorative color adds to the product value as well.

The coating performance depends mostly on the film hardness and the adhesive strength. Among the PVD processes, ion plating is a technique that can provide excellent adhesion strength and coatings of high hardness [9]. Therefore, reactive ion-plated TiN coatings have become popular in industry because of their ease of application and reliable performance. In the present study, hollow cathode discharge ion-plating (HCD-IP) was chosen as the coating method. Based on the results of earlier Taguchi experiments [10,11] and single-variable experiments on bias and nitrogen partial pressure [12,13], the deposition conditions were selected and single variable experiments on the film thickness were performed. The aim of this study is to investigate the effect of film thickness on the structure and mechanical properties of TiN coating on AISI 304 stainless steel.

2. Experimental details

The substrate material used in this study was mirror-polished 304 stainless steel with a composition of 0.1% Cu, 0.14%Co, 0.44%Si, 1.18% Mn, 8.73% Ni, 18.57% Cr, and the balance being Fe. Prior to the coating process, the specimens underwent ultrasonic cleaning progressively in acetone and ethanol and then dried in a vacuum dryer. The coating process was carried out in an HCD-IP system. The schematic diagram of the system is shown in Fig. 1.

Before deposition, the substrates were gradually heated to a temperature of 300°C. Meanwhile, the coating chamber was evacuated to 8.0×10^{-4} Pa to avoid the contamination in the coating process. Prior to deposition, the substrate surface was sputtered cleaned by Ar ions for 10 min at a pressure of 10.7 Pa Ar and 250 V substrate bias voltage. The evaporation of the Ti source by the electron beam was initiated by introducing 133–266 Pa of Ar and maintaining the gun power at 6 kW. A bias voltage of 40 V was applied to the substrate. After 1 min, the working gas consisting of 0.16 Pa of Ar and 0.13 Pa of nitrogen was introduced. The coating conditions of all samples were the same except that the deposition durations were varied to control the film thickness.

The crystal structure of the TiN films was identified by X-ray diffraction (XRD). The Cu $K\alpha$ line at 0.15405 nm was used as the source for diffraction. The XRD analysis was focused on the determination of (111) preferred orientation and residual stress. The extent of (111) preferred orientation is quantified by a texture coefficient $=I(111)/[I(111)+I(200)]$, where I is the integrated intensity of the corresponding Bragg peak.

The residual stress of TiN films was determined by the well-known XRD $\sin^2\psi$ method [14,15] using high precision 4-circle Huber diffractometer with psi-goniometer geometry. The Cu $K\alpha$ radiation was also used in this measurement. The existence of (111) preferred orientation in the TiN films made residual stress measurements difficult because the intensity of the high 2θ planes was too low for measurement. Best signal to noise ratio was found for the TiN (220) lattice plane at $2\theta=61.86°$, especially when the thickness of the film was below 600 nm. The (220) lattice plane was selected to derive the variation of lattice parameter among different ψ ?angles.

The thickness of each TiN film and the composition depth profile were measured by SIMS. Rutherford backscattering spectroscopy (RBS) was used to determine the N/Ti ratio and the atomic packing density. The N/Ti ratio was obtained from the RBS simulation equation.

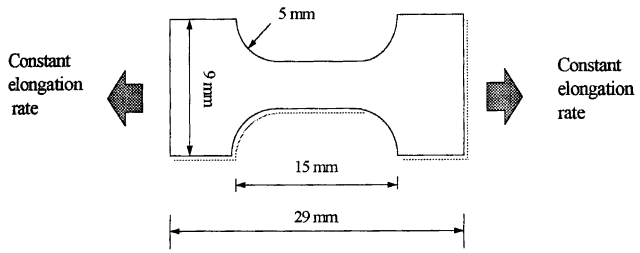

Fig. 2. The dimensions of the TiN coated specimen for the in-situ strip tension test.

After Rutherford backscattering experiment, the spectrum of the backscattering yield at different energy can be obtained. Using the Rump simulation code to simulate the spectrum, the N/Ti ratio can be acquired. The simulated atomic packing density (SAD) can also be obtained from the simulation results. Using the SAD value, the TiN film density can be determined by the following equation,

$$\text{Simulated film density (SD)} = \frac{SAD \times 10^{15}}{N_0 \times t/A},$$

where $SAD \times 10^{15}$ is the simulated atomic packing density ($\#/\text{cm}^2$), N_o is Avogadro number 6.02×10^{23}, t is the film thickness (cm), and A is the molecular weight of TiN (g/mol). From the results of the simulated film density, the packing factors of TiN films can be calculated as

$$\text{Packing Factor} = \frac{SD}{BD}$$

Where *SD* is the simulated film density, *BD* is the bulk density of TiN (g/cm^3).

Since large substrate effect may occur in the TiN films coated on AISI 304 stainless steel when using normal microhardness tester, the hardness was measured using a nanoindenter. To evaluate the creep effect, the load pattern was first increased linearly from 0 to the maximum load in 5 s, staying at the maximum load for 5 s and then releasing the load linearly from the maximum load to 0 in 5 s. The applying loads were ranging from 1000 to 4000 μN, depending on the depth displacement that should be less than one-tenth of the film thickness. For each sample, ten measurements were performed and the average value was reported.

The ultimate interfacial shear stress was determined by periodic cracking method based on in-situ strip tension of the TiN-coated specimens in a scanning electron microscope (SEM) chamber [16–18]. Fig. 2 illustrates the dimension of the specimen used in the in-situ strip tension test. The detail of the experimental procedures has been described elsewhere [18].

3. Results and discussion

The RBS results show that N/Ti ratios are consistently kept at a constant value of 0.8. The thicknesses of the TiN films were measured from the SIMS depth profile, and the results are listed in Table 1. Fig. 3 shows the variation of the packing factor with the thickness of TiN film. The packing factor increases linearly when the film thinner than 1μm, and levels off at 0.98 as thickness above 1.2 μm.

The hardness of the TiN film coated on 304 stainless steel was measured using a nanoindenter. Considering the indentation size effect, the load of the indenter was chosen to limit the penetration depth less than one tenth of the film thickness in order to minimize the effect of substrate on hardness of the thin film. Fig. 4 shows the variation of the hardness with the film thickness. The nanohardness values are ranging from 14.9 to 33.6 GPa. The hardness values of the samples S3 to S5 are all above 32 GPa, which seems to be very high for TiN coatings compared with previously reported data, mostly less than 25 GPa [3,19,20]. To confirm the hardness, a quartz standard sample was used to calibrate the nanoindenter, and the accuracy of the hardness was within 5%. In addition, ten indentations were made and the average

Table 1
Summary of the experimental results

Specimen no.	Thickness μm	Texture coefficient	N/Ti ratio GPa (load μN)	Hardness	Packing factor	Residual stress GPa	Apparent ultimate shear stress GPa	Corrected ultimate shear stress GPa
S1	0.22	0.51	0.8	14.9 (1000)	0.62	−5.93	–	–
S2	0.32	0.69	0.8	24.5 (2000)	0.65	−4.12	–	–
S3	0.75	0.70	0.8	33.6 (4000)	0.84	−3.12	6.93	6.26
S4	1.24	0.81	0.8	32.4 (4000)	0.98	−2.78	5.70	4.87
S5	1.68	0.85	0.8	32.1 (4000)	0.99	−2.7	5.61	4.82

(Deposition condition: gun power 6 kW; Ar pressure 0.16 Pa; N_2 pressure 0.13 Pa; substrate temperature 300°C.)

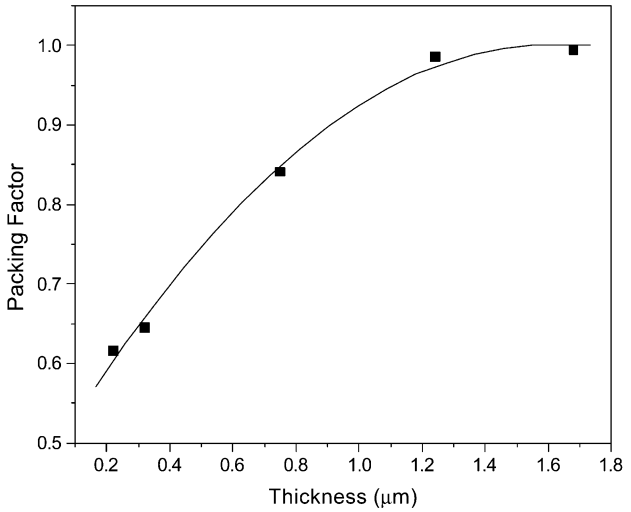

Fig. 3. Packing factor vs. film thickness for TiN deposited on 304 stainless steel.

value was reported. The precision of each value is within 10%. From Fig. 4, a general trend is observed that the hardness of TiN increases with the film thickness. The hardness rapidly increased as thickness varied from 0.32 to 0.75 μm and saturated to a value of approximately 33 GPa.

Fig. 5 shows the XRD diffraction patterns of all the TiN coated samples, with 2θ?scanning from 34° to 45°. The TiN (111) preferred orientation obviously increases and the corresponding (111) γ-Fe peak of the stainless steel decreases with increasing film thickness. Fig. 6 depicts the variation of texture coefficient with the film thickness. It is found that the texture coefficient increases with increasing film thickness, especially when the film thickness is greater than 1 μm, the (111) preferred orientation appears to be more pronounced. Fig. 7 shows

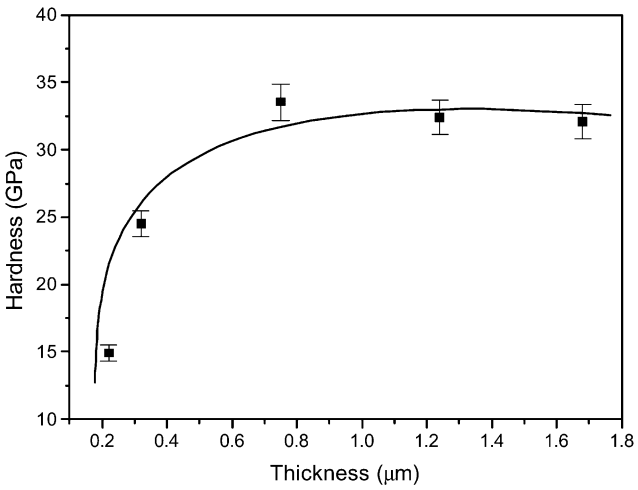

Fig. 4. Hardness varies with the film thickness for TiN deposited on 304 stainless steel.

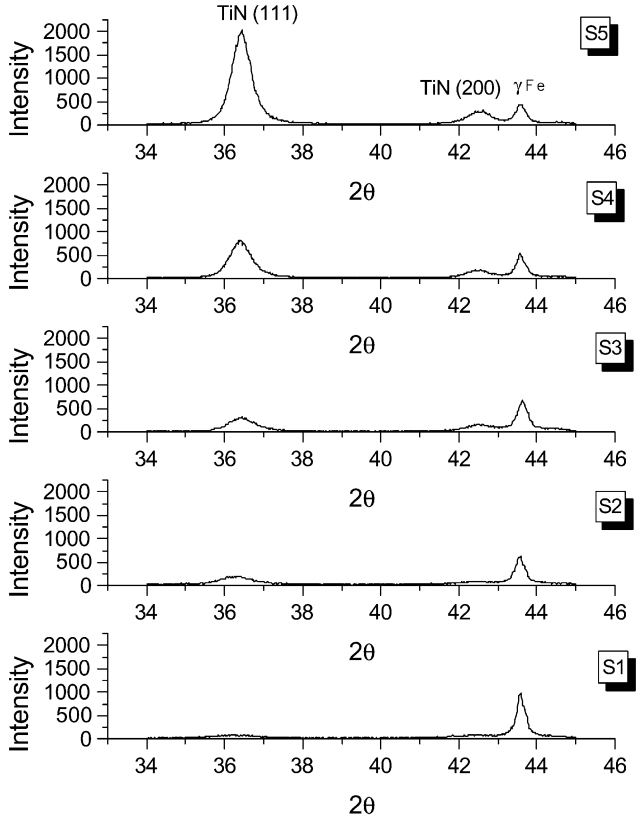

Fig. 5. The results of XRD, scanning from 2?=34° to 45° with different thickness.

the variation of the film hardness with the texture coefficient. The hardness increases as the (111) texture coefficient increases, especially as the texture coefficient above 0.7, the hardness rapidly increases to a saturated value.

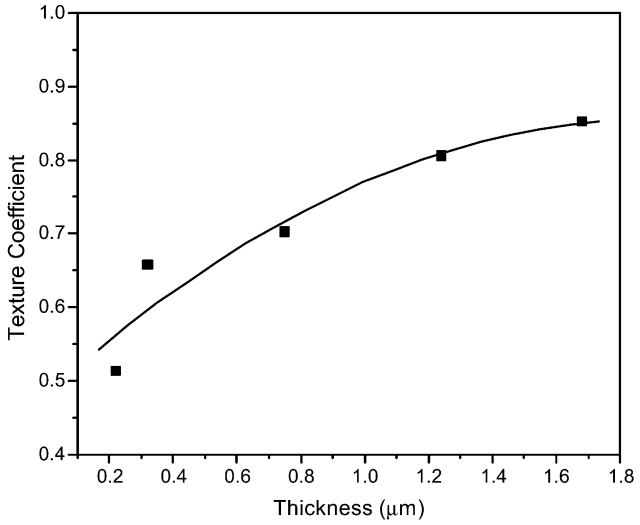

Fig. 6. The variation of the texture coefficient with the film thickness.

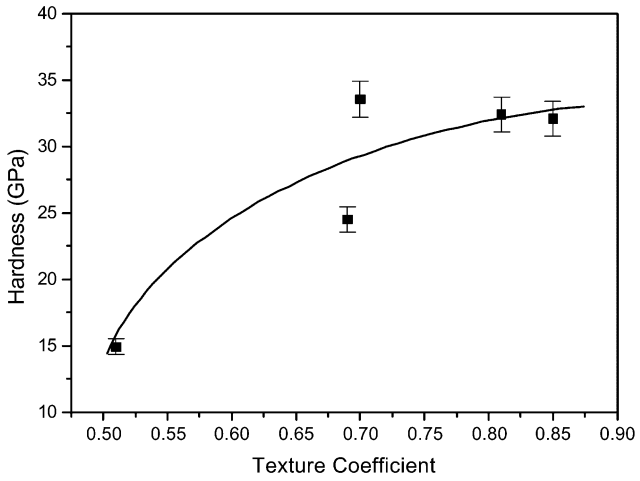

Fig. 7. The variation of the film hardness with the texture coefficient.

From the experimental results, it is found that the hardness of TiN films changes with a few factors; namely, the film thickness, the texture coefficient and the packing factor. Comparing Fig. 3, Fig. 4 and Fig. 7, one can find that these three figures all have the similar trend that hardness increases with the increasing factors such as film thickness, (111) texture coefficient or packing factor. From Fig. 4 the hardness increases from 14.9 to 33.6 GPa with increasing film thickness. Since the testing loads were chosen to keep the depth of indentation to be less than 1/10 of the film thickness, the substrate effect on the hardness values is minimized. Therefore, the increase of hardness is not supposed to be from the decrease of substrate effect as the film thickness increases.

Fig. 7 shows that the hardness increases with increasing (111) texture coefficient. Similar results have been reported by our previous study [4]. They explained the phenomenon by the relationship between (111) preferred orientation and the resolved shear stress on the slip systems of TiN. Since TiN has a NaCl-type structure, the active slip system of TiN is {110} ⟨110⟩ [21]. If the external force is perpendicular to the (111) plane, the resolved shear stress on all the slip systems is zero. Consequently, it is very difficult to induce plastic deformation, and thus higher hardness is measured. Therefore, if the film possesses a highly (111) preferred orientation, the hardness is higher than those of other orientations. It can be seen from Fig. 3 and Fig. 4 that the hardness increases with increasing packing factor. The packing factor represents the ratio of the film density to the theoretical density of TiN bulk material (5.39 g/cm^3). Increase of the packing factor means that the film was more close-packed and thereby having higher hardness. In summary, the film hardness is apparently influenced by the film thickness; however, since the packing factor and texture coefficient are also changed with the film thickness (Fig. 3 and Fig. 6), the effective parameters that affect the film hardness are texture coefficient and packing factor.

The residual stress data were collected via (220) diffraction peaks from a Cu Kα?source. The results of the residual stress in TiN films were listed in Table 1. The Poisson's ratio and Young's modulus, which are required for the calculation, were 0.21 [22] and 447 GPa [3], respectively. It is known that using $\sin^2\Psi$ method in textured material may encounter difficulties in residual stress measurement [15], and the accuracy of the results may not be as good as that of random sample. However, in the present study, the purpose for the measurement of residual stress is to know the variation of residual stress with the film thickness and therefore it is more concerned with precision than accuracy. The precision of the measurement can be seen from the relationship between lattice spacing and $\sin^2\Psi$. The results show that the (220) lattice plane spacing varies linearly with $\sin^2\Psi$, and the linear correlation coefficients are higher than 0.98 for all samples. Therefore, the precision of the measurements is satisfied for the purpose of this study. The residual stresses of the samples are ranging from −5.93 to −2.70 GPa. Fig. 8 shows the variation of the residual stress with the film thickness. It can be seen that the compressive residual stress decreases with increasing film thickness. Similar phenomenon was reported in ZrN film [23], and the residual stress was ranging from −4.8 to −3 GPa for the corresponding film thickness from 50 to 500 nm. It is speculated that the decreasing residual stress may be related to the increasing extent of (111) preferred orientation with film thickness. It has been reported that the formation of (111) preferred orientation in TiN is due to the fact that the elastic constant at ⟨111⟩ direction is smaller than that in ⟨200⟩ direction [5,6] and consequently, the strain is relaxed as the (111) preferred

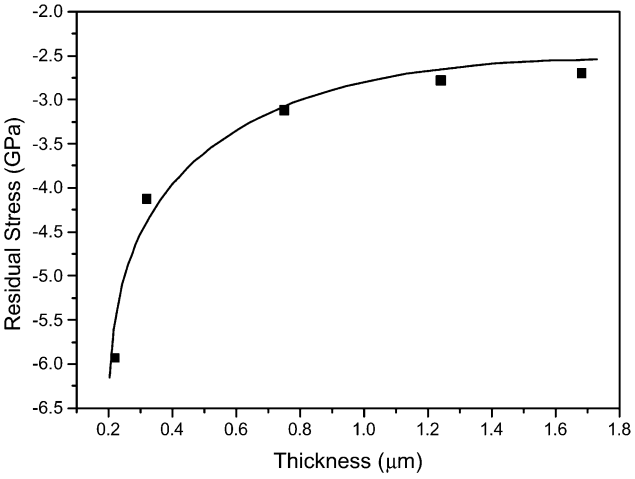

Fig. 8. The variation of residual stress with the film thickness.

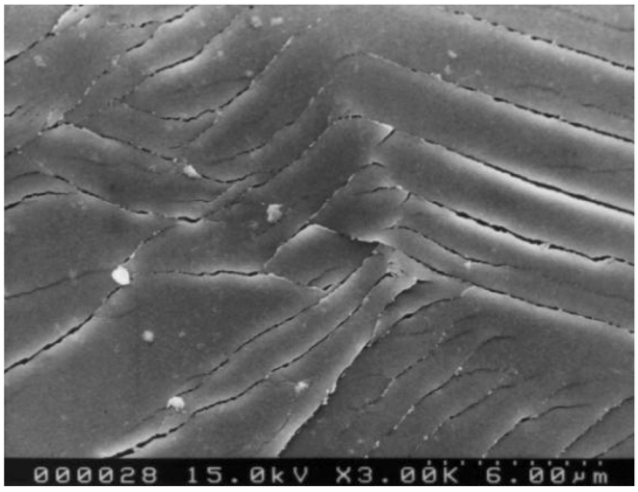

Fig. 9. The surface morphology of the specimens S1 after in-situ strip tension test. The tension force was applied in horizontal direction.

orientation becomes distinct. However, without further study, no proper explanation can be provided at the present stage.

The ultimate interfacial shear stress of TiN films can be discussed in two parts, the apparent ultimate interfacial shear stress and the corrected ultimate interfacial shear stress in which the residual stress was deducted. The ultimate interfacial shear stress, τ_{uss}, at the interface has been shown as [24,25]

$$\tau_{\mathrm{uss}} = \frac{\pi \cdot \delta \cdot \sigma_f}{\lambda_{\max}} \quad (1)$$

where σ_f is the fracture stress of the thin film, δ is the film thickness and $\lambda_{\max}$ is the maximum crack spacing in the thin film. Considering the residual stres of the thin film, our previous work [18] proposed the corrected ultimate shear stress, τ_{cuss}, at the interface is

$$\tau_{cuss} = \frac{\pi \cdot \delta \cdot \sigma_f}{\lambda_{\max}} \quad (2)$$

where $\sigma_e = \sigma_f + \sigma_r$ is the effective fracture stress and σ_r is the residual stress of the thin film. The results of the apparent and corrected ultimate interfacial shear stress according to Eq. (1) and Eq. (2) are listed in the Table 1, respectively.

Fig. 9 and Fig. 10 depict the surface morphology of the specimens S1 and S4 after in-situ strip tension test, respectively. Comparing Fig. 9 with Fig. 10, one can find that the cracks in Fig. 9 are not perpendicular to the tensile direction, which is different from that shown in Fig. 10. This phenomenon does not fulfill the basic requirement of the periodic cracking method, and consequently the ultimate interfacial shear stress of S1 cannot be determined. The cracking surface of specimen S2 shows the similar phenomenon that the cracks are irregular and centralized to some weak points. It is observed from Fig. 9 that the TiN coating is bulged in the central part and the cracks propagate to both sides. This is possibly due to the fact that the film is delaminated during strip-tension test. Once the film is detached from the substrate, the compressive residual stress presses the film and leads to the bulge.

When the film becomes thicker, the surface cracking behavior changes. Specimens S3 to S5 all show the similar surface crack pattern, cracks are perpendicular to the tensile direction, as shown in Fig. 10. Therefore the ultimate interfacial shear stress can be determined by the periodic cracking method. From this set of experiments, it is found that the minimum thickness of TiN film on which periodic cracking method can be applied effectively is approximately 0.5 μm.

4. Conclusions

1. The hardness of TiN films apparently increases with increasing film thickness and the effective factors that affect the film hardness are the texture coefficient and the packing factor.
2. The (111) preferred orientation and the packing factor of the TiN film increases with the film thickness.
3. The residual stress of TiN films is ranging from −5.93 to −2.70 GPa and decreases with increasing film thickness.
4. The ultimate interfacial shear stresses of the TiN/304SS specimens after the correction of residual stress are ranging from 4.82 to 6.26 GPa. The limiting thickness for the effective measurement of interfacial shear strength by the periodic cracking method is approximately 0.5 μm.

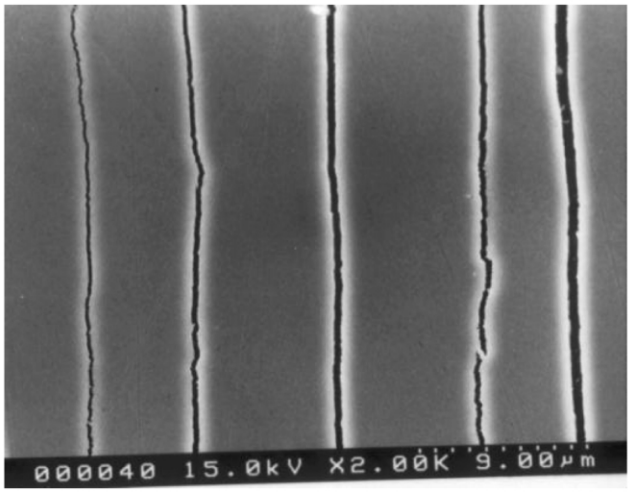

Fig. 10. The surface morphology of the specimens S4 after in-situ strip tension test. The tension force was applied in horizontal direction.

Acknowledgements

This research was funded by the National Science Council of the Republic of China under the contracts NSC 89-2216-E-007-036 and NSC 88-3011-B-007-001-NU. Residual stress measurement was carried out in the Department of Materials Science and Engineering, University of Illinois. Nanoindentation was carried out in the Center for Microanalysis of Materials, Frederick Seitz Materials Research Laboratory, University of Illinois. The authors would like to thank Mr. Cheng-Hsin Ma, for his help in residual stress and nanoindentation measurements.

References

[1] H. Ljungcrantz, M. Oden, L. Hultman, J.E. Greene, J.-E. Sundgren, J. Appl. Phys. 80 (1996) 6725.
[2] B.O. Johansson, J.-E. Sundgren, J.E. Greene, A. Rockett, S.A. Barnett, J. Vac. Sci. Technol. A 3 (2) (1985) 303.
[3] H. Ljungcrantz, M. Oden, L. Hultman, J.E. Greene, J.-E. Sundgren, J. Appl. Phys. 80 (1996) 6725.
[4] C.T. Chen, Y.C. Song, G.-P. Yu, J.-H. Huang, J. Mater. Eng. Perform. 7 (1998) 324.
[5] J.H. Je, D.Y. Noh, H.K. Kim, K.S. Liang, J. Appl. Phys. 81 (9) (1997) 6126.
[6] J. Pelleg, L.Z. Zevin, S. Lungo, N. Croitora, Thin Solid Films 197 (1991) 117.
[7] F. Hohl, H.-R. Stock, P. Mayr, Surf. Coat. Technol. 54/55 (1992) 160.
[8] W.R. LaFontaine, C.A. Paszkiet, M.A. Korhonen, C.-Y. Li, J. Mater. Res. 6 (10) (1991) 2084.
[9] N.A.G. Ahmed, Ion Plating Technology: Developments and Applications, Wiley, New York, 1987.
[10] W-L Pan, G-P Yu, J-H Huang, Surf. Coat. Technol. 110 (1998) 111.
[11] B.F. Chen, W.L. Pan, G.P. Yu, J. Hwang, J.H. Huang, Surf. Coat. Technol. 111 (1999) 16.
[12] J.-H. Huang, Y.-P. Tsai, G.-P. Yu, Thin Solid Films 440 (1999) 355–356.
[13] J-Y Chen, G-Pi Yu, J-H Huang, Mater. Chem. Phys. 65 (2000) 310.
[14] E. Macherauch, P. Müller, Z. Angw, Physik 13 (1961) 305.
[15] I.C. Noyan, J.B. Cohen, Residual Stress: Measurement by Diffraction and Interpretation, Springer-Verlag, New York, 1987.
[16] F.S. Shieu, L.H. Cheng, Y.C. Sung, J.H. Huang, G.P. Yu, Mater. Chem. Phys. 50 (1997) 248.
[17] F.S. Shieu, L.H. Cheng, Y.C. Sung, J.H. Huang, G.P. Yu, Thin Solid Films 334 (1998) 125.
[18] B.F. Chen, J. Hwang, G.P. Yu, J.H. Huang, Thin Solid Films 352 (1999) 173.
[19] E. Vancoille, J.P. Celis, J.R. Roos, Thin Solid Films 224 (1993) 168.
[20] M. Larsson, M. Bromark, P. Hedenqvist, S. Hogmark, Surf. Coat. Technol. 202 (1995) 76–77.
[21] L. Hultman, M. Shinn, P.B. Mirkarimi, S.A. Barnett, J. Cryst. Growth 135 (1994) 309.
[22] J.O. Kim, J.D. Achenbach, P.B. Mirkarimi, M. Shinn, S.A. Barnett, J. Appl. Phys. 72 (1992) 1805.
[23] P Jin, S Maruno, Jpn. J. Appl. Phys. 30 (1991) 1463.
[24] D.C. Agrawal, R. Raj, Acta Metall. 37 (1989) 1265.
[25] F.S. Shieu, R. Raj, S.L. Sass, Acta Metall. Mater. 38 (1990) 2215.